Author Manuscript

Author Manuscript

Author Manuscript

Author Manuscript

HHS Public Access

Author manuscript

Cancer Res. Author manuscript; available in PMC 2023 October 16.

Published in final edited form as:

Cancer Res. 2018 June 01; 78(11): 2966–2977. doi:10.1158/0008-5472.CAN-17-2269.

Mutant IDH1 Cooperates with ATRX Loss to Drive the Alternative Lengthening of Telomere Phenotype in Glioma

Joydeep Mukherjee[1], **Tor-Christian Johannessen**[2], **Shigeo Ohba**[3], **Tracy T. Chow**[4], **Lindsey Jones**[1], **Ajay Pandita**[5], **Russell O. Pieper**[1]

[1]Department of Neurological Surgery, University of California, San Francisco, San Francisco, California.

[2]The Kristian Gerhard Jebsen Brain Tumor Research Centre, Department of Biomedicine, University of Bergen, Bergen, Norway.

[3]Department of Neurosurgery, Fujita Health University, Toyoake, Aichi, Japan.

[4]Department of Biochemistry and Biophysics, University of California, San Francisco, San Francisco, California.

[5]Core Diagnostics, Hayward, California.

Abstract

A subset of tumors use a recombination-based alternative lengthening of telomere (ALT) pathway to resolve telomeric dysfunction in the absence of TERT. Loss-of-function mutations in the chromatin remodeling factor ATRX are associated with ALT but are insufficient to drive the process. Because many ALT tumors express the mutant isocitrate dehydrogenase IDH1 R132H, including all lower grade astrocytomas and secondary glioblastoma, we examined a hypothesized role for IDH1 R132H in driving the ALT phenotype during gliomagenesis. In p53/pRb–deficient human astrocytes, combined deletion of ATRX and expression of mutant IDH1 were sufficient to create tumorigenic cells with ALT characteristics. The telomere capping complex component RAP1 and the nonhomologous DNA end joining repair factor XRCC1 were each downregulated consistently in these tumorigenic cells, where their coordinate reexpression was sufficient to suppress the ALT phenotype. RAP1 or XRCC1 downregulation cooperated with ATRX loss in driving the ALT phenotype. RAP1 silencing caused telomere dysfunction in ATRX-deficient

Corresponding Author: Russell O. Pieper, University of California, San Francisco, 1450 S. 3rd St, HD492, San Francisco, CA 94143-0520. Phone: 415-502-7132; Fax: 415-502-8376; rpieper@cc.ucsf.edu.

Authors' Contributions

Conception and design: J. Mukherjee, T.-C. Johannessen, S. Ohba, R.O. Pieper

Development of methodology: J. Mukherjee, T.-C. Johannessen, S. Ohba, T.T. Chow, A. Pandita, R.O. Pieper

Acquisition of data (provided animals, acquired and managed patients, provided facilities, etc.): J. Mukherjee, T.-C. Johannessen, S. Ohba, T.T. Chow, L. Jones, A. Pandita, R.O. Pieper

Analysis and interpretation of data (e.g., statistical analysis, biostatistics, computational analysis): J. Mukherjee, T.-C. Johannessen, T.T. Chow, R.O. Pieper

Writing, review, and/or revision of the manuscript: J. Mukherjee, T.-C. Johannessen, S. Ohba, R.O. Pieper

Administrative, technical, or material support (i.e., reporting or organizing data, constructing databases): J. Mukherjee

Study supervision: R.O. Pieper

Supplementary data for this article are available at Cancer Research Online (http://cancerres.aacrjournals.org/).

Disclosure of Potential Conflicts of Interest

No potential conflicts of interest were disclosed.

Author Manuscript Author Manuscript Author Manuscript Author Manuscript

cells, whereas XRCC1 silencing suppressed lethal fusion of dysfunctional telomeres by allowing IDH1-mutant ATRX-deficient cells to use homologous recombination and ALT to resolve telomeric dysfunction and escape cell death. Overall, our studies show how expression of mutant IDH1 initiates telomeric dysfunction and alters DNA repair pathway preferences at telomeres, cooperating with ATRX loss to defeat a key barrier to gliomagenesis.

Significance: Studies show how expression of mutant IDH1 initiates telomeric dysfunction and alters DNA repair pathway preferences at telomeres, cooperating with ATRX loss to defeat a key barrier to gliomagenesis and suggesting new therapeutic options to treat low-grade gliomas.

Introduction

A rate-limiting step in the development of most cancers is the resolution of telomeric dysfunction. Telomeres are DNA–protein complexes that protect chromosomes ends from being erroneously recognized as damaged DNA. Telomeric DNA is elongated by TERT-mediated reverse transcription of a TERC RNA template (1). TERT expression is silenced during development, and human somatic cells forced to divide in the absence of TERT fail to fully replicate the ends of chromosomes, losing 50 to 200 bp of telomeric DNA per cell division (2). When the telomeric DNA becomes critically short, the six-protein component of the telomere, known as the shelterin cap, dissociates (3). The resulting exposed telomeric end activates DNA double-strand break (DSB) repair pathways that cause cell-cycle arrest and senescence in normal cells, or the fusion of telomeres and chromosomal instability that leads to the death of most cells that cannot undergo cell-cycle arrest (4). Telomeric dysfunction therefore limits the continued growth of TERT-deficient cells, making resolution of telomere shortening critical for oncogenesis.

Most tumors solve the problem of shortening telomeres by either never silencing TERT expression, or by acquiring mutations that reactivate the silenced TERT promoter (5). Approximately 10% to 15% of tumors, in contrast, do not reactivate TERT expression. Rather these tumors, which include small percentages of various solid tumors, 50% of chondrogenic tumors, and virtually all lowergrade astrocytoma (LGA) and secondary glioblastoma (6) use an alternative, homologous recombination (HR)–based mechanism to elongate telomeres, reestablish telomere capping, and escape cell death in the absence of TERT (7). This so-called alternative lengthening of telomere (ALT) mechanism remains a relatively poorly understood process by which telomeric DNA on one chromosomal arm is used as a template for DNA polymerase-mediated, TERT-independent extension of shortened telomeres on a different arm (8). The recombination and interchromosomal copying leads to three phenotypic hallmarks of ALT: telomere–associated protein aggregates known as ALT-associated promyelocytic leukemia bodies (APB) where recombination occurs; intermediates of recombination, including extrachromosomal circles of single-stranded telomeric DNA (C-circles); and telomeric sister chromatid exchange (T-SCE) generated by the transfer of telomeric sequence from one chromatid to another (9). These characteristics, along with the heterogeneously long telomeres that result from the ALT process (9), have helped define the ALT phenotype both *in vitro* and in tumors *in vivo*.

Author Manuscript Author Manuscript Author Manuscript Author Manuscript

Although the characteristics of the ALT phenotype are well defined, the factors driving the process are less so. ALT is uniformly associated with loss-of-function mutations in the histone chaperone ATRX, and ATRX alterations are a common surrogate marker of the ALT phenotype (10, 11). ATRX associates with sites of histone H3K9 trimethylation, facilitates telomeric H3.3 deposition, and suppresses telomeric HR (12, 13). Consistent with these functions, introduction of ATRX into ATRX-mutant ALT fibroblasts reduces levels of APBs, C-circles, and T-SCEs (14). The deletion of *ATRX* in nonglial cells, however, is insufficient to induce the ALT phenotype or to lead to cellular transformation (14), suggesting that other factors likely contribute to the generation of ALT.

The human tumors in which ALT is most common are also those most likely to contain mutations in IDH1 (6, 15). R132H *IDH1* mutations occur early in the development of glioma and encode a mutant IDH1 protein that dimerizes with wild-type (WT) IDH1 (16). The IDH1-mutant/WT dimer displays a neomorphic activity that converts α-ketoglutarate (αKG) to 2-hydroxyglutarate (2-HG; ref. 17). 2-HG in turn accumulates and competes with αKG for binding to a wide variety of αKG–dependent dioxygenases (18). The end result is the inhibition of multiple enzymes involved in the control of DNA cytosine methylation and histone methylation (19, 20) and widespread changes in gene expression (21). Furthermore, we and others have shown that expression of mutant IDH1 is sufficient to transform p53/pRb–deficient immortalized human astrocytes, further supporting the causative role mutant IDH1 plays in gliomagenesis (21-25). Of note, in LGA, the overlap between IDH1 mutation, loss-of-function *ATRX* mutation, and ALT is essentially 100% (7), suggesting that IDH1 mutation may in some way collaborate with *ATRX* loss to efficiently resolve telomeric dysfunction in otherwise TERT-deficient cells, and set the stage for gliomagenesis.

To address this possibility, we employed an *in vitro* gliomagenesis model developed in our laboratory and most recently used to help define the role of mutant IDH1 in gliomagenesis (21, 23-26). In this system mortal, TERT-negative human astrocytes are rendered p53- and pRb-deficient by introduction of the viral proteins E6 and E7, after which other genetic alterations can be introduced and monitored for effects on cellular processes, including immortalization and transformation. Using this system, as well as xenograft cells from IDH1-mutant human glioma, we here define a pathway by which mutant IDH1 induces telomeric dysfunction, alters the processing of dysfunctional telomeres, and cooperates with ATRX mutations to drive the ALT phenotype and gliomagenesis.

Materials and Methods

Cell culture

SF10602 cells were provided by the UCSF Brain Tumor Center Tissue Core, BT142 cells were purchased from ATCC, GM847 were purchased from The Coriell Institute (Camden, NJ), and MGG119 human glioma cells were a gift from Daniel Cahill (Massachusetts General, Boston, MA). All cells were cultured as described previously (27, 28), and identities were confirmed by short tandem repeat analysis (Promega Geneprint Kit), confirmed *Mycoplasma* negative (MycoSensor Mycoplasma Detection PCR Assay Kit; Agilent Technologies), and used within 3 passages of thawing.

Author Manuscript Author Manuscript Author Manuscript Author Manuscript

Modulation of ATRX, IDH1, RAP1, and XRCC1 expression

CRISPR-based ATRX knockout—CRISPR-mediated ATRX knockout cells were generated from E6E7-expressing human astrocytes (25) using two guide RNAs (exon 7: 5′-ATTGTGAGCTCCACTGCTTGTGG-3′; exon 9: 5′-CAAAACATGTAAAAAAGTACAGG-3′) in a modified pX330A vector as described previously (29). Briefly, cells were transfected with 2 μg of vector, incubated at 37° C for 3 days, and then seeded in puromycin-containing DMEM media. Individual colonies that arose were then selected and expanded, and DNA was extracted and subjected to PCR-based genotyping using PCR primers that flanked the targeted deletion region between exons 7 and 9 in *ATRX* (forward, F: 5′ AATAATAGCCACTCCTTCTCCTAG-3; reverse, R: 5′-GTATGCAAAAATAAATAAAAAATTC-3′) and generated a single 7,500-bp band in control cells and a single 700-bp band in successful recombinants. All clones were analyzed for off-target CRISPR-based recombination as described previously (30).

Modulation of IDH1 mut, IDH1 WT, RAP1, and XRCC1—For overexpression studies, ATRX WT or ATRX-KO, E6E7-expressing human astrocytes were infected with blank lentiviral constructs or constructs encoding EGFP-tagged IDH1 mut (R132H) or IDH1 WT, subjected to FACS-based sorting after 120 hours, and then verified for target expression by Western blot analysis. The IDH1-expressing cells, or MGG119 cells, were further infected with blank lentiviral constructs or constructs encoding GFP-tagged RAP1 or RFP-tagged XRCC1, harvested after 72 hours, and verified for target expression by Western blot analysis. For transient expression studies, infection efficiency was estimated to be >90%.

For suppression studies, ATRX KO, IDH1 WT astrocytes were transiently transfected (Fugene 6) with nontargeted siRNA (scramble, Scr), or a pool of 5 different siRNAs targeting RAP1 or XRCC1 as described preciously (27). After 48 hours, suppression of target expression (>90%) was verified by Western blot analysis.

Analysis of protein and mRNA expression and telomerase activity

Western blot analysis was performed as described previously (27) using antibodies specific for ATRX (1:200), XRCC1 (1:250), Lig3 (1:250) (Santa Cruz Biotechnology), RAP1 (1:1,000, Sigma), pan IDH1, mutant IDH1R132H (Dianova), and β-actin (1: 20,000; Cell Signaling Technology). mRNA expression analysis was performed by quantitative PCR as described previously (Supplementary Table S1; ref. 31). Telomerase activity was measured using a TRAPeze Kit (Millipore).

Characterization of the ALT phenotype

APBs—Cells on 4-well chambered slides were fixed in paraformaldehyde, rinsed, blocked (3% normal goat serum and 0.2% Triton X-100 in PBS), and then incubated with promyelocytic leukemia body (PML) or TRF2 (1:200) primary antibodies in 1% goat serum and 0.2% Triton X-100 in PBS (18–20 hours, 4°C). After washing, slides were incubated with fluorescent-tagged secondary antibodies (647 or 488, respectively, 1:200, 2 hours, Invitrogen) appropriate for the host species of the primary antibody. Following washing, sections were incubated with DAPI, washed, and mounted. Negative controls for antibody labeling were performed by omitting primary or secondary antibodies, in which case, nuclei

Author Manuscript Author Manuscript Author Manuscript Author Manuscript

examined exhibited no fluorescence. Fluorescence microscopy was performed on >200 cells per group, with APBs defined as yellow foci resulting from overlap of PML and TRF2 signal.

T-SCE (CO-FISH)—CO-FISH was performed as described previously (32). Briefly, cells were incubated for 16 hours with bromodeoxyuridine, followed by colcemid for the last 2 hours. Following fixation, metaphase spreads were prepared on glass slides, incubated with RNase, stained with Hoechst 33258, and ultraviolet-treated before Exonuclease III digestion. Spreads were then formaldehyde fixed, treated with pepsin, fixated again followed by 70%, 90%, and 100% ethanol dehydration, and then incubated with the leading strand probe (TelC-Cy3-red, PNA Bio, 1.5 hours, 80°C). Slides were consecutively washed with formamide-based solution and PBS, dehydrated, and incubated with the lagging strand probe (TelG-FITC-green, PNA Bio) for another 1.5 hours. After similar washes, the slides were then dehydrated, DAPI-stained, and mounted for microscopy. Negative controls were performed by omitting the PNA probes, in which case nuclei examined exhibited no fluorescence. Yellow foci where the signal from the leading and lagging strand probes overlapped in an otherwise normal metaphase spread were considered to be representative of T-SCE events. The percentage of chromosomes exhibiting T-SCE in the equivalent of 50 cells per group was then quantitated.

C-circles—Levels of C-circles were determined as described previously (33). Briefly, various amounts of HinfI and RsaI-digested DNA from each cell group was subjected to amplification by phi29 polymerase, after which levels of amplified C-circle DNA were determined by immobilization on a membrane and hybridization to an end-labeled [AACCCT]4 telomeric oligonucleotide probe, or by quantitative PCR–based analysis using C-circle–specific primers (34). In each case, signal intensity derived from three independent DNA preparations for each cell group was normalized to levels in positive control GM847 fibroblasts.

Multiple telomeric signal and telomeric fusion—FISH was performed on metaphase spreads using a Cy3-labeled (CCCTAA)3 PNA oligonucleotide (Dako) as described previously (31), followed by DAPI counterstaining. FluoreSpheres fluorescent beads (Molecular Probes) used to monitor signal intensity loss during microscope use and negative controls were performed by omitting the PNA probes, in which case nuclei examined exhibited no fluorescence. Metaphase spreads from 50 cells were then counted in each cell group, and the number of chromosome arms with >1 telomeric signal per metaphase were determined. For telomeric fusion analysis, the percentage of metaphase spreads with ≥1 fused chromosomes (chromosomes with adjacent but not over-lapping signal) was determined.

Cell growth and colony formation assays

Cell number and colony formation efficiency were determined by trypan blue exclusion counting and colony formation assay as described previously (35, 36).

Author Manuscript Author Manuscript Author Manuscript Author Manuscript

Telomere dysfunction–induced foci analysis

Telomere dysfunction–induced foci (TIF) analysis was carried out as for APBs with the use of γH2AX- and TRF2 (1:200)-specific primary antibodies, and the fluorescent-tagged secondary antibodies. Fluorescence microscopy was performed on >200 cells per group, and the percentage of cells with TIFs (yellow foci resulting from overlap of gamma H2AX and TRF2 signal) was determined.

Statistical analysis

Data are reported as mean ± SE of at least three experiments. When two groups were compared, the unpaired Student t test was applied (*P* value). When multiple groups were evaluated, the one-way ANOVA test with *post hoc* Tukey–Kramer multiple comparisons test was used. $P < 0.05$ was considered statistically significant.

Results

Mutant IDH1 expression stimulates ALT-mediated resolution of telomeric dysfunction

To begin to assess the potential linkage between IDH1 mutation and ALT, we introduced mutant IDH1 and/or used CRISPR-based editing to genetically eliminate ATRX in TERT-negative human astrocytes rendered p53- and pRb-deficient by introduction of the viral proteins E6 and E7. The defective p53 and pRb signaling in these astrocytes mimics that noted in LGA (37), and in these cells (Fig. 1, Cont) neither the CRISPR-based, targeted homozygous deletion of *ATRX* (Fig. 1A and B, 2 independent clones ATRX KO-1 and KO-2 and Supplementary Fig. S1A) nor stable introduction of mutant IDH1 (+IDH1 mut, Fig. 1A and B) alone resulted in detectable levels of TERT mRNA (not shown) or TERT activity via TRAP analysis relative to positive control parental E6E7 cells exogenously expressing hTERT (Fig. 1C). Similarly, no control, ATRX-KO, or mutant IDH1–expressing cultures exhibited any signs of the ALT phenotype (APBs; Fig. 1D; Supplementary Fig. S1B), T-SCEs (Fig. 1E; Supplementary Fig. S1C), or C-circles (Fig. 1F; Supplementary Fig. S1D), relative to positive control GM847 fibroblasts known to display the ALT phenotype (38). Prolonged growth of the +IDH1 mut or ATRX KO cultures eventually led to cell crisis consistent with the lack of TERT activity in these cells. Although no ATRX-deficient cells survived, +IDH1mut clones emerged after 6 months in crisis, in each case associated not with ALT, but with reactivation of the WT TERT promoter (27). Thus, although expression of mutant IDH1 in the p53/pRb–deficient setting can over time facilitate reactivation of the WT TERT promoter, neither the loss of *ATRX*, nor mutant IDH1 expression alone drives ALT.

In contrast, combining genetic elimination of *ATRX* with exogenous expression of mutant IDH1 (Fig. 1A and B) resulted in TERT-negative cells (Fig. 1C) that exhibited ABPs, T-SCE, C-circles, and growth in soft agar (a hallmark of *in vitro* gliomagenesis; Fig. 1D-G; Supplementary Fig. S1B-S1E), without any detectable off-target CRISPR effects (Supplementary Fig. S1F). These data therefore represent the first indication that mutant IDH1 can contribute to gliomagenesis in part by stimulating ALT-mediated resolution of telomeric dysfunction.

Author Manuscript Author Manuscript Author Manuscript Author Manuscript

IDH1mut-mediated downregulation of RAP1 and XRCC1 is associated with ALT

Although the initial data showed that mutant IDH1 can help drive ALT, they did not provide any specific clues as to how this was accomplished. Because mutant IDH1 expression causes 2HG-mediated changes in gene expression, we used quantitative PCR to determine whether any of 40 genes encoding proteins involved in telomere biology was differentially expressed in IDH1mut, ATRX KO cells relative to matched cells with neither, or only one of these alterations. Two genes, *RAP1* and *XRCC1*, were consistently downregulated in the mutant IDH1–expressing cells regardless of cellular ATRX status (Fig. 2A, 8 representative genes; Supplementary Fig. S2A), perhaps consistent with the mutant IDH1–driven wide-scale CpG island methylation and gene silencing noted in these cells (27). The RAP1 and XRCC1 proteins were also downregulated in the mutant IDH1–expressing cells relative to control cells, as was DNA ligase 3 (Lig3), a protein stabilized by interaction with XRCC1 (Fig. 2B; ref. 39). RAP1, XRCC1, and Lig3 were similarly downregulated in IDH1-mutant, ATRX-mutant human glioma xenografts (BT142, SF10602, and MGG119), which display the ALT phenotype (Fig. 2B; Supplementary Fig. S2B-S2E; ref. 28). Furthermore, an analysis of The Cancer Genome Atlas database showed that mRNA expression levels of XRCC1 and RAP1 were both significantly reduced in histologically lower grade, mutant IDH1-expressing LGA and mixed oligoastrocytomas (relative to normal brain controls or GBM, Fig. 2C). These results suggest that expression of mutant IDH1, independently of ATRX status, downregulates the expression of proteins that play a role in telomere biology in glioma cells.

Mutant IDH1–mediated downregulation of RAP1 and XRCC1 drives the ALT phenotype

To examine whether mutant IDH1–driven downregulation of RAP1 and/or XRCC1 causes, rather than is merely associated with, the ALT phenotype, we transiently (72 hours) overexpressed RAP1, XRCC1, or RAP1 + XRCC1 in either of two independently derived IDH1mut, *ATRX*-KO astrocyte cultures that exhibited the ALT phenotype. Overexpression of either RAP1 or XRCC1 alone (Fig. 3A; Supplementary Fig. S3A) significantly reduced levels of APBs, T-SCE, C-circles (Fig. 3B-D; Supplementary Fig. S3B-S3D), and clonogenicity (Fig. 3E; Supplementary Fig. S3E), whereas expression of both RAP1 and XRCC1 led to further additive decreases comparable with those noted following reintroduction of ATRX (Fig. 3A-D; Supplementary Fig. S3A-S3D).

To address the potential linkage between mutant IDH1–driven downregulation of RAP1 and/or XRCC1 and ALT in human mutant IDH1–driven glioma xenograft cells, similar experiments were performed in MGG119 ATRX-mutant, IDH1-mutant human glioma cells that express both WT and mutant IDH1 and exhibit the ALT phenotype. As in the genetically modified astrocyte model, overexpression of either RAP1 or XRCC1 alone (Fig. 4A) significantly reduced levels of APBs, T-SCE, C-circles (Fig. 4B-D), cell viability (Fig. 4E), and clonogenicity (Fig. 4F) relative to the parental MGG119 cells, whereas expression of both RAP1 and XRCC1 caused additive decreases comparable with those noted following reintroduction of ATRX (Fig. 4A-F).

In converse experiments, two independently derived IDH1 WT, *ATRX*-deficient, non-ALT astrocyte cultures were transfected with a nontargeted siRNA (Scr) or siRNA pools targeting

Author Manuscript Author Manuscript Author Manuscript Author Manuscript

XRCC1 or RAP1, after which the ability of these alterations to substitute for mutant IDH1 in driving ALT in the *ATRX*-deficient background were monitored. siRNA-mediated downregulation of either RAP1 or XRCC1 alone (Fig. 5A; Supplementary Fig. S4A, lanes 2 and 3 vs. lane 1 siScr controls) caused significant increases in levels of APBs, T-SCE, C-circles (Fig. 5B-D; Supplementary Fig. S4B-S4D), and clonogenicity (Fig. 5E; Supplementary Fig. S4E), whereas downregulation of both RAP1 and XRCC1 led to further additive increases comparable with those noted following reintroduction of mutant IDH1 itself (Fig. 5A-E; Supplementary Fig. S4A-S4E). These studies therefore confirm that mutant IDH1 uses suppression of RAP1 and XRCC1 to drive ALT and gliomagenesis.

Mutant IDH1–mediated downregulation of RAP1 initiates telomere dysfunction

Because RAP1 is part of the shelterin complex that protects chromosome ends from being recognized as DNA damage (40), we considered the possibility that RAP1 downregulation, in combination with loss of ATRX, caused telomeric dysfunction that initiated ALT. To address this possibility, we first monitored the appearance of γH2AX foci that colocalized with a telomere-specific probe (TIFs), as a sign of response to telomeric damage. Control p53/pRb–deficient astrocytes exhibited γH2AX foci indicative of generalized low-level DNA DSBs, but few cells exhibited γH2AX foci at telomeres (TIFs, Fig. 6A). The same was true for p53/pRb–deficient astrocytes either expressing mutant IDH1 or having lost *ATRX*. IDH1mut, ATRX-KO ALT astrocytes, however, exhibited TIFs, a sign of response to persistent telomeric dysfunction (Fig. 6A). Furthermore, another sign of telomere damage [the number of chromosome arms with >1 telomeric signal (red) per metaphase spread; ref. 41] was also significantly increased in the IDH1mut, *ATRX*-KO ALT astrocytes relative to p53/pRb–deficient astrocytes either expressing mutant IDH1 or having lost *ATRX* (Supplementary Fig. S5A). Although exogenous expression of XRCC1 had a minimal effect on the percentage of ATRX KO-1/IDH1 mut cells exhibiting TIFs, overexpression of RAP1 in these cells significantly suppressed TIF formation (Fig. 6B). Conversely, the downregulation of RAP1, but not of XRCC1, in IDH WT, *ATRX*-KO astrocytes also resulted in the appearance of TIFs (Fig. 6C), suggesting that in the *ATRX* KO background, suppression of RAP1 was sufficient to induce telomeric dysfunction and in part drive the ALT phenotype.

IDH1mut-mediated downregulation of XRCC1 facilitates ALT by altering telomeric damage repair

Although XRCC1 contributes to repair of DNA single-strand breaks (40), it is also a critical component of the alternative nonhomologous end joining (aNHEJ) pathway in which it stabilizes DNA ligase 3 and allows the direct religation of DNA DSBs (42). aNHEJ acts on some (but not all) forms of dysfunctional telomeres to yield fatal, end-to-end chromosomal fusions (43). Mutant IDH1–driven downregulation of XRCC1 may therefore limit the fusion of dysfunctional telomeres and allow alternative pathways, and perhaps HR to resolve telomere dysfunction. Consistent with this idea, the overexpression of XRCC1 that suppressed the hallmarks of ALT in IDH1mut, *ATRX*-deficient astrocytes (Fig. 3) at the same time also increased the levels of NHEJ-mediated telomeric fusion, which in turn was also associated with decreased cell viability (Fig. 6D; Supplementary Fig. S5B). Similar results were noted in MGG119 ALT cells following XRCC1 overexpression (Fig. 6E). These

Author Manuscript Author Manuscript Author Manuscript Author Manuscript

results suggest that mutant IDH1, by suppressing levels of XRCC1, lessens the degree to which NHEJ can be used to fuse dysfunctional telomeres and eliminate ATRX-deficient cells from the population. The suppression of XRCC1-mediated NHEJ in turn appears to indirectly or directly free cells to use HR to act upon mutant IDH1–induced dysfunctional telomeres and generate the ALT phenotype (Fig. 6F).

Discussion

The ALT mechanism is an important process used by a select group of human cancers to resolve telomeric dysfunction and maintain unlimited growth potential. The process is poorly understood and to date has only been linked to the loss of TERT and ATRX function, neither or which alone or in combination induces the ALT phenotype. The current study shows that expression of mutant IDH1, which is among the earliest and most common alterations in ALT-associated glioma, cooperates with *ATRX* loss to facilitate telomeric dysfunction, alter the processing of dysfunctional telomeres, and drive the ALT phenotype.

Mutant IDH1 appears to contribute to the generation of the ALT in glioma cells in at least two critical ways. First, the mutant IDH1–mediated downregulation of RAP1 contributes to the generation of dysfunctional telomeres. In this study, RAP1 was the only member of the telomere-protective shelterin complex whose expression was significantly downregulated by mutant IDH1 expression. Downregulation of RAP1 causes telomeric dysfunction and the appearance of TIFs in some systems (40), but not in others (44). In our study, RAP1 downregulation led to the appearance of TIFs in the context of ATRX loss, suggesting that the two cooperate under normal conditions to maintain telomere capping. Consistent with this finding, telomere dysfunction induced by downregulation of other shelterin components, such as TPP1, also induces ALT in the *ATRX*-deficient setting (45). The dysfunctional telomeres induced by mutant IDH1–driven RAP1 downregulation do not bind 53BP1 (not shown) and as such do not appear to exist in a "fully uncapped" state (46). They are, however, sufficiently altered to initiate a DNA damage response (although not cell-cycle arrest in these checkpoint-deficient cells) and to be susceptible to NHEJ and chromosomal fusion upon reexpression of XRCC1. Mutant IDH1 expression in the ATRX-deficient setting therefore appears to provide cells with a unique opportunity to modify telomere architecture.

Mutant IDH1 also appears to contribute to ALT by downregulating XRCC1 and altering the balance between pathways that process dysfunction telomeres. XRCC1 is a critical component of the aNHEJ pathway that fuses DNA ends with minimal sequence homology (42). Furthermore, aNHEJ lethally fuses some forms of dysfunctional telomeres (43), although this has not been examined in the ATRX-deficient setting. Mutant IDH1–mediated downregulation of XRCC1 and the aNHEJ pathway may therefore limit the removal of cells with dysfunctional telomeres and make cells more reliant on pathways such as HR that could favor survival by resolving telomeric dysfunction in less lethal ways. Mutant IDH1–driven downregulation of RAP1, a proven suppressor of HR (47), may further this process. Although cells expressing mutant IDH1 have been suggested to be relatively deficient in both NHEJ and HR (48), cells transformed by mutant IDH1 expression retain enough HR to repair temozolomide-induced DNA DSB (24) and perform ALT, suggesting

Author Manuscript Author Manuscript Author Manuscript Author Manuscript

that sub-maximal levels of HR may be sufficient to drive recombination in the appropriate circumstances.

Although the abovementioned findings provide the first link between mutant IDH1 expression and ALT, this linkage is clearly context dependent. Many IDH1 WT, SV40-transformed fibroblast cell lines exhibit the ALT phenotype (9). Conversely virtually all lower grade oligodendrogliomas exhibit IDH1 mutations, yet few, if any, display ATRX mutations or ALT (10). Mutant IDH1 expression can also, in the absence of ATRX mutations, facilitate reactivation of the endogenous WT TERT promoter (26). It may therefore be that ALT requires an exact series of events that includes a generalized induction of telomere dysfunction coupled with alterations in DNA repair pathways that favor HR. Although this can be brought about experimentally by deletion of shelterin components, such as TRF2 and/or POT1, in a NHEJ (ligase 4)-deficient background (49), LGAs appear to reach this same endpoint simply by combining mutant IDH1–driven downregulation of RAP1 and XRCC1 with loss-of-function ATRX mutations. Conversely, in the absence of ATRX mutations, mutant IDH1 expression may favor other forms of telomeric extension, including TERT promoter reactivation (26). Other underlying predis-positions, however, may also exist, as may differences in cells of origin that favor certain forms of resolution of telomeric dysfunction over others.

The abovementioned findings not only have implications for our understating of the ALT phenotype, but also for the therapy of ALT tumors. The data suggest that mutant IDH1–driven ALT tumors exist in a state of persistent telomere dysfunction resolved only by suppression of XRCC1 and a shift from aNHEJ to HR. Although targeting of mutant IDH1 maybe a rational therapeutic approach, IDH1 mutant–driven changes in gene expression do not appear to be reversible outside a narrow window of time (24). Furthermore, the ALT phenotype induced by mutant IDH1 expression in the current study was not reversed by mutant IDH1 inhibitors (not shown), suggesting that other approaches may be needed. Inhibitors of HR may also be reasonable, although these agents are not at the stage of clinical testing. Alternatively, agents that directly or indirectly facilitate NHEJ, and perhaps cNHEJ, could prove useful in the mutant IDH1–driven ALT setting. The suggestion that the action of PARP inhibitors involves stimulation of cNHEJ (50) may in this regard be worth investigating.

Supplementary Material

Refer to Web version on PubMed Central for supplementary material.

Acknowledgments

We thank Daniel P. Cahill and Hiroki Wakimoto for the MGG119 cell line. T. T. Chow was supported by the Damon Runyon Cancer Research Foundation (DRG-2168-13). This work was supported in part by NIH GrantCA172845-03 (to R.O. Pieper), the Loglio Research Project (to R.O. Pieper), and The Kristian Gerhard Jebsen Foundation and The Norwegian Cancer Society (to T.-C. Johannessen).

Author Manuscript Author Manuscript Author Manuscript Author Manuscript

References

1. Greider CW. Telomerase and telomere-length regulation: lessons from small eukaryots to mammals. Cold Spring Harb Symp Quant Biol 1993; 58:719–23. [PubMed: 7525147]
2. Muraki K, Nyhan K, Han L, Murnane J. Mechanisms of telomere loss and their consequences for chromosome instability. Front Oncol 2012;2:135. [PubMed: 23061048]
3. Palm W, de Lange T. How shelterin protects mammalian telomeres. Annu Rev Genet 2008;42:301–34. [PubMed: 18680434]
4. Lazzerini-Denchi E, Sfeir A. Stop pulling my strings-what telomeres taught us about the DNA damage response. Nat Rev 2016;17:364–78.
5. Eckel-Passow JE, Lachance DH, Molinaro AM, Walsh KM, Decker PA, Sicotte H, et al. Glioma groups based on 1p/19q, IDH, and TERT promoter mutations in tumors. N Engl J Med 2015;372:2499–508. [PubMed: 26061753]
6. Heaphy CM, Subhawong AP, Hong SM, Goggins MG, Montgomery EA, Gabrielson E, et al. Prevalence of the alternative lengthening of telomeres maintenance mechanism in human cancer subtypes. Am J Path 2011;179:1608–15. [PubMed: 21888887]
7. Ceccarelli M, Barthel FP, Malta TM, Sabedot TS, Salama SR, Murray BA, et al. Molecular profiling reveals biologically discrete subsets and pathways of progression in diffuse glioma. Cell 2016;164:550–63. [PubMed: 26824661]
8. Cesare AJ, Reddel RR. Alternate lengthening of telomeres: models, mechanisms and implications. Nat Rev Genet 2010;11:319–30. [PubMed: 20351727]
9. Henson JD, Reddel RR. Assaying and investigating alternative lengthening of telomeres activity in human cells and cancers. FEBS Lett 2010;584:3800–11. [PubMed: 20542034]
10. Killela PJ, Reitman ZJ, Jiao Y, Bettegowda C, Agrawal N, Diaz LA Jr, et al. TERT promoter mutations occur frequently in gliomas and a subset of tumors derived from cells with low rates of self-renewal. Proc Natl Acad Sci U S A 2013;110:6021–6. [PubMed: 23530248]
11. Schwartzentruber J, Korshunov A, Liu XY, Jones DT, Pfaff E, Jacob K, et al. Driver mutations in histone H3.3 and chromatin remodelling genes in paediatric glioblastoma. Nature 2012;482:226–31. [PubMed: 22286061]
12. Xue Y, Gibbons R, Yan Z, Yang D, McDowell TL, Sechi S, et al. The ATRX syndrome protein forms a chromatin-remodeling complex with Daxx and localizes in promyelocytic leukemia nuclear bodies. Proc Natl Acad Sci U S A 2003;100:10635–40. [PubMed: 12953102]
13. Ritchie K, Seah C, Moulin J, Isaac C, Dick F, Bérubé NG. Loss of ATRX leads to chromosome cohesion and congression defects. J Cell Biol 2008;180:315–24. [PubMed: 18227278]
14. Napier CE, Huschtscha LI, Harvey A, Bower K, Noble JR, Hendrickson EA, et al. ATRX represses alternate lengthening of telomeres. Oncotarget 2015;6:16543–58. [PubMed: 26001292]
15. Lu C, Venneti S, Akalin A, Fang F, Ward PS, DeMatteo RG, et al. Induction of sarcomas by mutant IDH2. Genes Dev 2013;27:1986–98. [PubMed: 24065766]
16. Jin G, Reitman ZJ, Duncan CG, Spasojevic I, Gooden DM, Rasheed BA, et al. Disruption of wild-type IDH1 suppresses D-2-hydroxyglutarate production in IDH1-mutated gliomas. Cancer Res 2013;73:496–501. [PubMed: 23204232]
17. Ward PS, Patel J, Wise DR, Abdel-Wahab O, Bennett BD, Coller HA, et al. The common feature of leukemia-associated IDH1 and IDH2 mutations is a neomorphic enzyme activity converting alpha-ketoglutarate to 2-hydroxyglutarate. Cancer Cell 2010;17:225–34. [PubMed: 20171147]
18. Xu W, Yang H, Liu Y, Yang Y, Wang P, Kim S-H, et al. Oncometabolite 2-hydroxyglutarate is a competitive inhibitor of α-ketoglutarate-dependent dioxygenases. Cancer Cell 2011;19:17–30. [PubMed: 21251613]
19. Sasaki M, Knobbe CB, Munger JC, Lind EF, Brenner D, Brustle A, et al. IDH1 (R132H) mutation increase murine haematopoietic progenitors and alters epigenetics. Nature 2012;488:656–9. [PubMed: 22763442]
20. Barski A, Cuddapah S, Cui K, Roh TY, Schones DE, Wang Z, et al. High-resolution profiling of histone methylations in the human genome. Cell 2007;1294:823–37.

Author Manuscript Author Manuscript Author Manuscript Author Manuscript

21. Lu C, Ward PS, Kapoor GS, Rohle D, Turcan S, Abdel-Wahab O, et al. IDH1 mutation impairs histone demethylation and results in a block to cell differentiation. Nature 2012;483:474–8. [PubMed: 22343901]
22. Turcan S, Rohle D, Goenka A, Walsh LA, Fang F, Yilmaz E, et al. IDH1 mutation is sufficient to establish the glioma hypermethylator phenotype. Nature 2012;483:479–83. [PubMed: 22343889]
23. Ohba S, Mukherjee J, See WL, Pieper RO. Mutant IDH1-driven cellular transformation increases RAD51-mediated homologous recombination and temozolomide resistance. Cancer Res 2014;74:4836–44. [PubMed: 25035396]
24. Johannessen TA, Mukherjee J, Viswanath P, Ohba S, Ronen SM, Bjerkvig R, et al. Rapid conversion of mutant IDH1 from driver to passenger in amodel of human gliomagenesis. Mol Cancer Res 2017;14:976–83.
25. Sonoda Y, Ozawa T, Hirose Y, Aldape KD, McMahon M, Berger MS, et al. Formation of intracranial tumors by genetically modified human astrocytes defines four pathways critical in the development of human anaplastic astrocytoma. Cancer Res 2001;61:4956–60. [PubMed: 11431323]
26. Ohba S, Mukherjee J, Johannessen T-C, Mancini A, Chow TT, Wood M, et al. Mutant IDH1 expression drives TERT promoter reactivation as part of the cellular transformation process. Cancer Res 2016;76:6680–9. [PubMed: 27758882]
27. Tateishi K, Wakimoto H, Iafrate AJ, Tanaka S, Loebel F, Lelic N, et al. Extreme vulnerability of IDH1 mutant cancers to NAD+ depletion. Cancer Cell 2015;28:673–84.
28. Wakimoto H, Tanaka S, Curry WT, Loebel F, Zhao D, Tateishi K, et al. Targetable signaling pathway mutations are associated with malignant phenotype in IDH-mutant gliomas. Clin Cancer Res 2014;20:2898–909. [PubMed: 24714777]
29. Ran FA, Hsu PD, Wright J, Agarwala V, Scott DA, Zhang F. Genome engineering using CRISPR-Cas9 system. Nat Protoc 2012;9:2281–308.
30. Hsu PD, Scott DA, Weinstein JA, Ran FA, Konermann S, Agarwala V, et al. DNA targeting specificity of RNA-guided Cas9 nucleases. Nat Biotechnol 2013;31:827–32. [PubMed: 23873081]
31. Mukherjee J, Phillips JJ, Zheng S, Wiencke J, Ronen SM, Pieper RO. Pyruvate kinase M2 expression, but not pyruvate kinase activity, is up-regulated in a grade-specific manner in human glioma. PLoS One 2013;8:e57610. [PubMed: 23451252]
32. Ourliac-Garnier I, Londono-Vallejo A. Telomere strand-specific length analysis by fluorescent in situ hybridization (Q-CO-FISH). Methods Mol Biol 2011;735:33–46. [PubMed: 21461809]
33. Henson JD, Cao Y, Huschtscha LI, Chang AC, Au AY, Pickett HA, et al. DNA C-circles are specific and quantifiable markers of alternative-lengthening-of-telomeres activity. Nat Biotechnol 2009;27:1181–5. [PubMed: 19935656]
34. Lau LMS, Dagg RA, Henson JD, Au AYM, Royds JA, Reddel RR. Detection of alternative lengthening of telomeres by telomere quantitative PCR. Nuc Acids Res 2013;41:e34–43.
35. See WL, Tan IL, Mukherjee J, Nicolaides T, Pieper RO. Sensitivity of glioblastomas to clinically available MEK inhibitors is defined by neurofibromin 1 deficiency. Cancer Res 2012;72:3350–9. [PubMed: 22573716]
36. Mirzoeva OK, Kawaguchi T, Pieper RO. The Mre11/Rad50/Nbs1 complex interacts with the mismatch repair system and contributes to temozolomide-induced G2 arrest and cytotoxicity. Mol Can Ther 2006;5:2757–66.
37. Okana S, Lan L, Caldecott KW, Mori T, Yasui A. Spatial and temporal cellular responses to single-strand breaks in human cells. Mol Cell Biol 2003;23:3974–81. [PubMed: 12748298]
38. Bryan TM, Englezou A, Gupta J, Bacchetti S, Reddel RR. Telomere elongation in immortal human cells without detectable telomerase activity. EMBO J 1995;14:4240–8. [PubMed: 7556065]
39. Caldecott KW, McKeown CK, Tucker JD, Ljungquist S, Thompson LH. An interaction between the mammalian DNA repair protein XRCC1 and DNA ligase III. Mol Cell Biol 1994;14:68–77. [PubMed: 8264637]
40. Benarroch-Popivker D, Pisano S, Mendez-Bermudez A, Lototska L, Kaur P, Bauwens S, et al. TRF2-mediated control of telomere DNA topology as a mechanism for chromosome end protection. Mol Cell 2016;61:274–86. [PubMed: 26774283]

Author Manuscript Author Manuscript Author Manuscript Author Manuscript

41. Sfeir A, Kosiyatrakul ST, Hockemeyer D, MacRae SL, Karlseder J, Schildkraut CL, et al. Mammalian telomeres resemble fragile sites and require TRF1 for efficient replication. Cell 2009;138:90–103. [PubMed: 19596237]

42. Audebert M, Salles B, Calsou P. Involvement of poly (ADP-ribose) polymerase-1 and XRCC1/DNA ligase III in an alternative route for DNA double-strand breaks rejoining. J Biol Chem 2004;279:55117–26. [PubMed: 15498778]

43. Doksani Y, de Lange T. Telomere-internal double-strand breaks are repaired by homologous recombination and PARP1/Lig3-dependent end-joining. Cell Rep 2016;17:1646–56. [PubMed: 27806302]

44. Kabir S, Hockemeyer D, de Lange T. TALEN Gene knockouts reveal no requirement for the conserved human shelterin protein Rap1 in telomere protection and length regulation. Cell Rep 2014;9:1273–80. [PubMed: 25453752]

45. Hu Y, Shi G, Zhang L, Li F, Jiang Y, Jiang S, et al. Switch telomerase to ALT mechanism by inducing telomeric DNA damages and dysfunction of ATRX and DAXX. Sci Rep 2016;6:32280–8. [PubMed: 27578458]

46. Cesare A, Karlseder J. A three-state model of telomere control over human proliferative boundaries. Curr Opin Biol 2012;24:731–8.

47. Sfeir A, Kabir S, van Overbeek M, Celli GB, deLange T. LossofRap1 induces telomere recombination in absence of NHEJ or a DNA damage signal. Science 2010;327:1657–61. [PubMed: 20339076]

48. Sulkowski PL, Corso CD, Robinson ND, Scanlon SE, Pushouse KP, Bai H, et al. 2-Hydroxyglutarate produced by neomorphic IDH mutations suppresses homologous recombination and induces PARP inhibitor sensitivity. Sci Transl Med 2017;9:eaal2463. [PubMed: 28148839]

49. Deng Y, Guo X, Ferguson DO, Chang S. Multiple roles for MRE11 at uncapped telomeres. Nature 2009;460:914–8. [PubMed: 19633651]

50. Patel AG, Sarkaria JN, Kaufman SH. Nonhomologous end joining drives poly(ADP-ribose) polymerase (PARP) inhibitor lethality in homologous recombination-deficient cells. Proc Natl Acad Sci U S A 2011;108:3406–11. [PubMed: 21300883]

Author Manuscript Author Manuscript Author Manuscript Author Manuscript

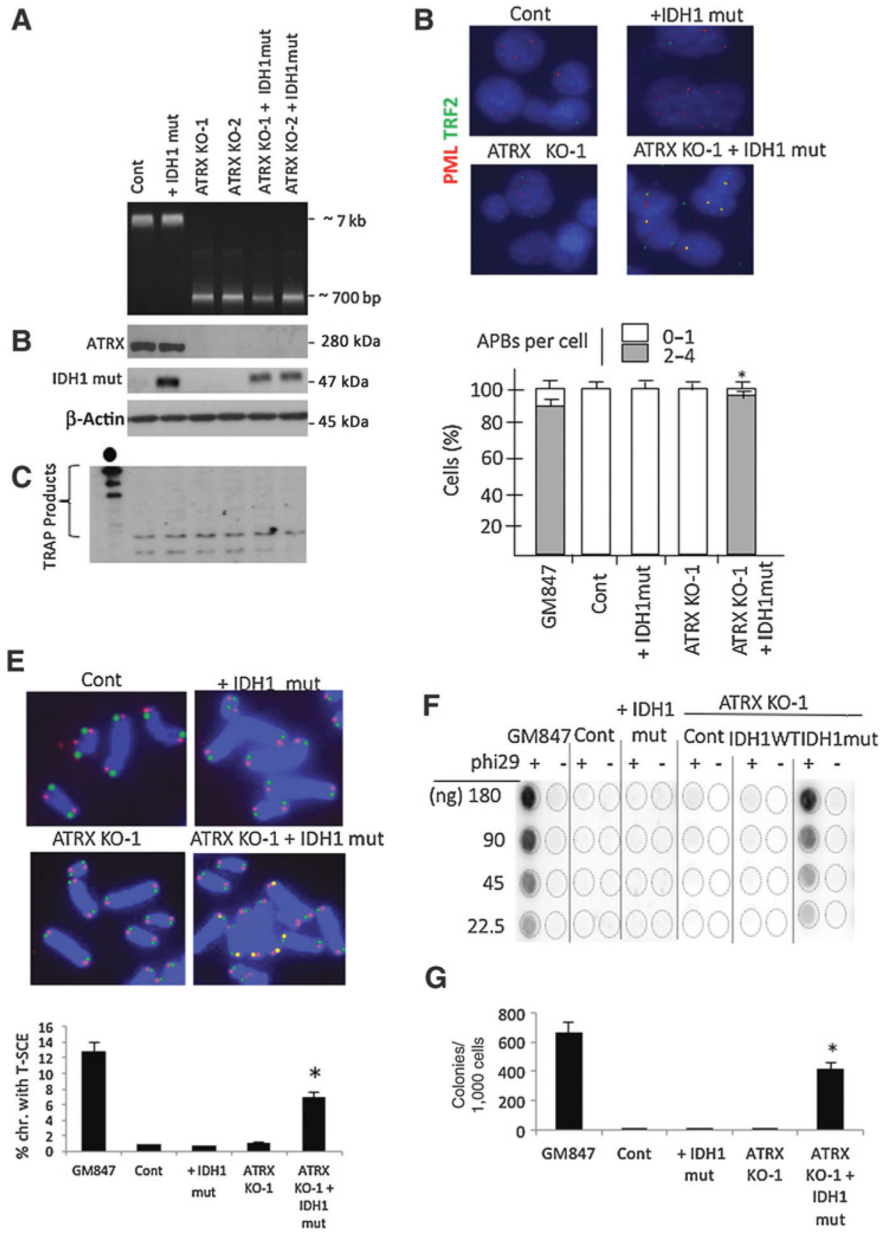

Figure 1.

Mutant IDH1 cooperates with ATRX loss to stimulate ALT. **A,** PCR-based analysis of DNA from E6E7-expressing human astrocytes (Cont) exogenously expressing mutant IDH1 (+mutIDH1), subjected to CRISPR-based homozygous deletion of *ATRX* (ATRX KO-1 and ATRX KO-2), or both yields a 700-bp product in cells having undergone successful homozygous deletion of *ATRX* exons 7–9. **B,** Western blot verification of ATRX, mutant IDH1, and β-actin expression in cells in **A**. **C,** TRAP analysis of telomerase activity in cells in **A** and in control E6E7 astrocytes exogenously expressing hTERT (leftmost lane, closed circle). **D,** Quantitation of the percentage of cells containing ≤1 (open box) or 2–4 (closed box) APBs per cell (bottom) based on IHC colocalization (yellow foci) of PML (red) with TRF2 (green) signal (top) in DAPI-stained (blue) positive-control GM847 ALT cells and the

Author Manuscript Author Manuscript Author Manuscript Author Manuscript

ATRX-KO1–based cells in **A**. $N \geq 200$ cells per group. **E,** Quantitation of the percentage of chromosomes with T-SCE (bottom) based on fluorescence colocalization of leading (red)- and lagging (green)–strand telomeric probes (top) in >50 cells per ATRX-KO1-based cells in **A**. **F,** Quantitation of C-circle DNA following amplification of varying amounts of genomic DNA from GM847 and ATRX KO-1–based cells in **A** in reactions with (+) or without (−) phi29 polymerase that were spotted (dotted areas) and hybridized to a telomeric G strand-specific probe. **G,** Number of colonies (>100 cells) that arose 28 days following plating of the ATRX KO-1–based cells in **A** in soft agar. Except where noted, all values were derived from three independent experiments. *, $P < 0.05$.

Author Manuscript Author Manuscript Author Manuscript Author Manuscript

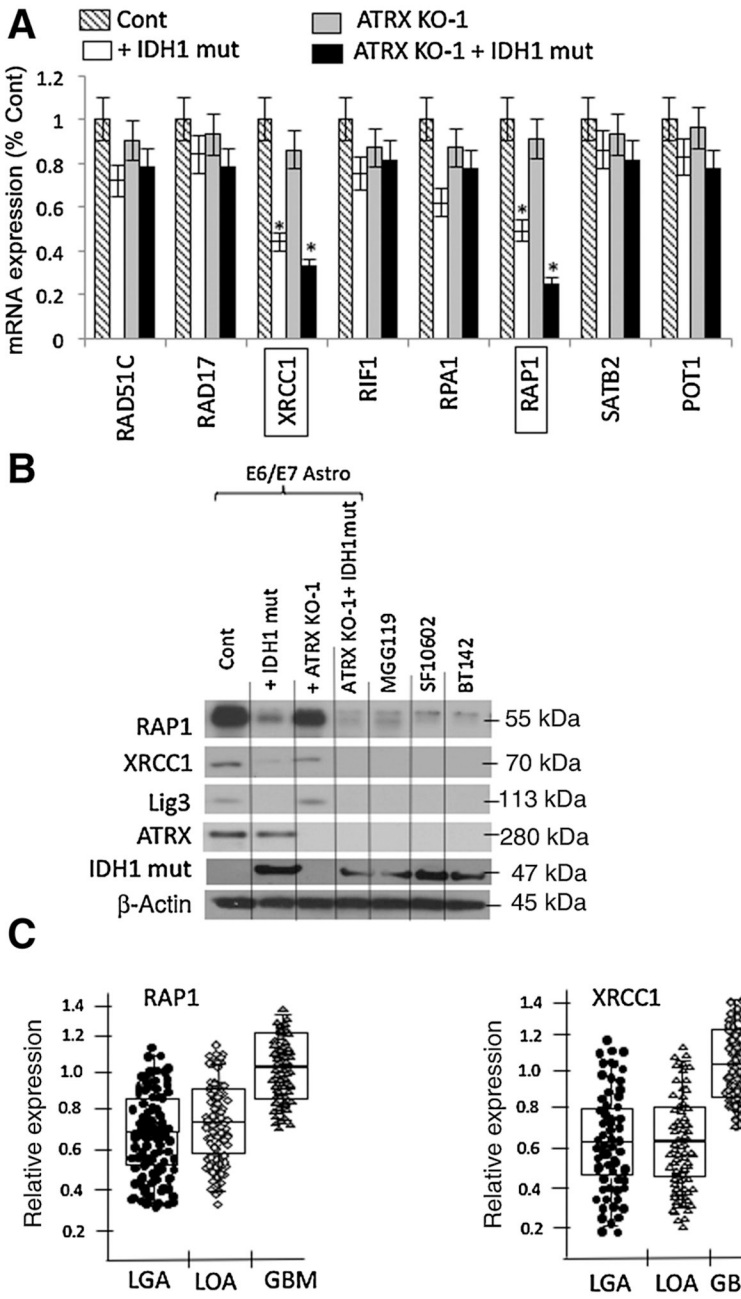

Figure 2.

Mutant IDH1 expression is associated with downregulation of RAP1 and XRCC1. **A,** Triplicate quantitative PCR analysis of the levels of select transcripts encoding proteins involved in telomere regulation in control cells (E6E7 astrocytes) expressing mutant IDH1, subjected to CRISPR-based deletion of *ATRX*, or both. **B,** Western blot analysis of RAP1, XRCC1, DNA ligase 3 (Lig3), and β-actin protein levels in the cells in **A** and in BT142, SF10602, and MGG119 IDH1-mutant ALT glioma cells. **C,** The Cancer Genome Atlas–based analysis of XRCC1 and RAP1 mRNA levels in LGA, lower-grade mixed oligoastroglioma (LOA), and GBM relative to normal brain controls (1.0 on the *y*-axis). *, $P < 0.05$.

Author Manuscript Author Manuscript Author Manuscript Author Manuscript

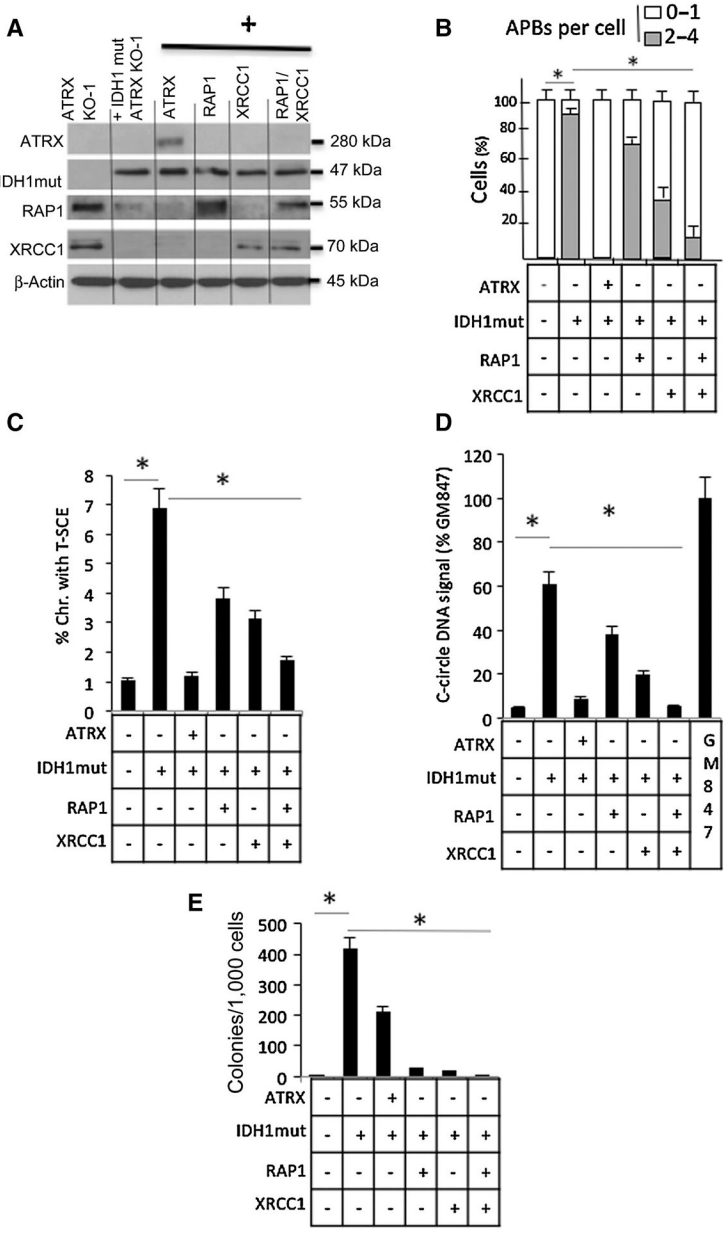

Figure 3.

Forced overexpression of RAP1 and/or XRCC1 suppresses mutant IDH1-mediated ALT phenotype in genetically modified human astrocytes. **A,** Western blot verification of ATRX, mutant IDH1, RAP1, XRCC1, and β-actin protein levels in *ATRX* KO-1 astrocytes, and *ATRX* KO-1 astrocytes exogenously expressing mutant IDH1 plus ATRX, RAP1, XRCC1, or both RAP1 and XRCC1. **B,** Quantitation of the percentage of cells from **A** containing ≤1 (open box) or 2–4 (closed box) APBs per cell. $N \geq 200$ cells per group. ATRX (−), CRISPR-based deletion of ATRX, ATRX (+), exogenous re-introduction of ATRX. **C,** Percentage of chromosomes with T-SCE in cells from **A**. **D,** PCR-based quantification of C-circle signal (relative to that in positive control GM847 ALT fibroblasts) following phi29-mediated amplification of genomic DNA (30 ng) from cells in **A**. **E,** Number of colonies (>100 cells)

Author Manuscript Author Manuscript Author Manuscript Author Manuscript

that arose 28 days following plating of the cells in **A**. Except where noted, all values were derived from three independent experiments. *, $P < 0.05$.

Author Manuscript Author Manuscript Author Manuscript Author Manuscript

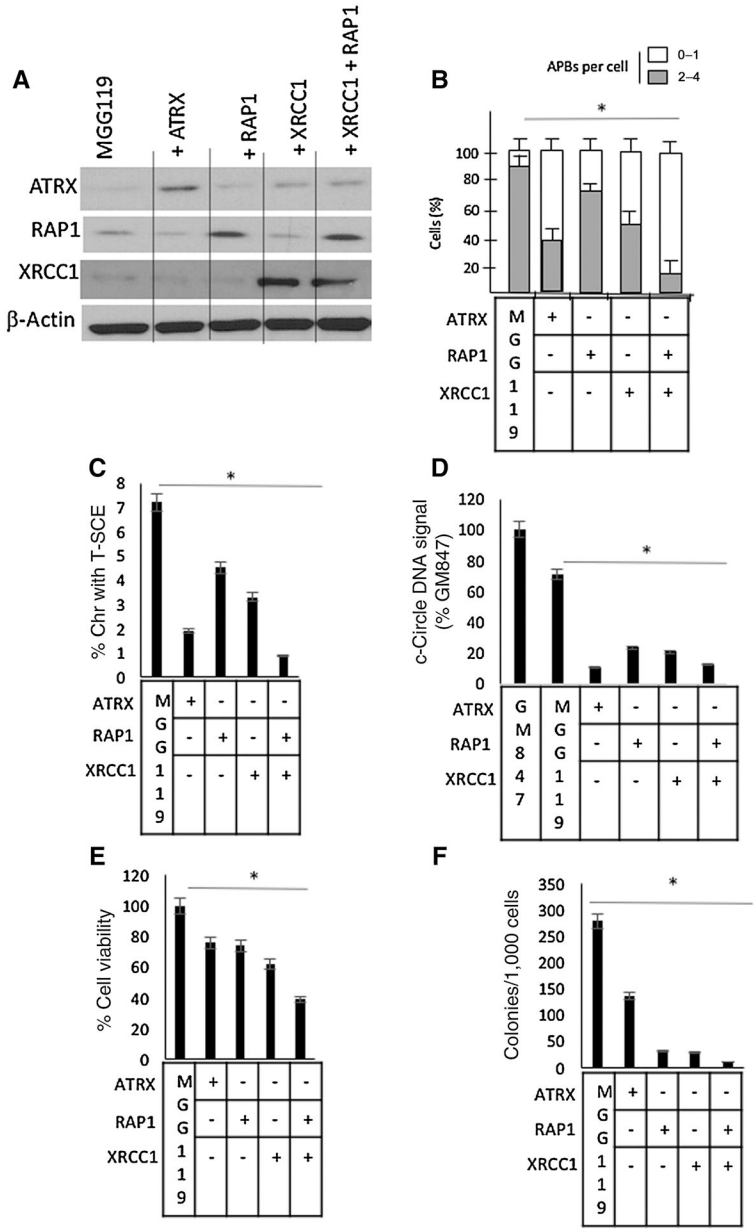

Figure 4.

Forced overexpression of RAP1 and/or XRCC1 suppresses mutant IDH1–mediated ALT phenotype in ATRX-deficient, mutant IDH1, ALT MGG119 xenograft cells. **A,** Western blot verification of ATRX, RAP1, XRCC1, and β-actin protein levels in MGG119 cells, and the same cells exogenously expressing ATRX, RAP1, XRCC1, or both RAP1 and XRCC1. **B,** Quantitation of the percentage of cells containing ≤1 (open box) or 2–4 (closed box) APBs per cell in >200 cells per each group described in **A**. +/− symbols denote the exogenous introduction of ATRX, RAP1, or XRCC1 (+), or of blank vector (−). **C,** Percentage of chromosomes with T-SCE in cells in **A**. **D,** PCR-based quantification of C-circle signal (relative to that in positive control GM847 ALT fibroblasts) following phi29-mediated amplification of genomic DNA (30 ng) from cells in **A**. **E,** Viability of cells in **A** measured

Author Manuscript Author Manuscript Author Manuscript Author Manuscript

by trypan blue exclusion. **F,** Number of colonies (>100 cells) that arose 28 days following plating of the cells in **A**. Except where noted, all values were derived from three independent experiments. *, $P < 0.05$.

Author Manuscript Author Manuscript Author Manuscript Author Manuscript

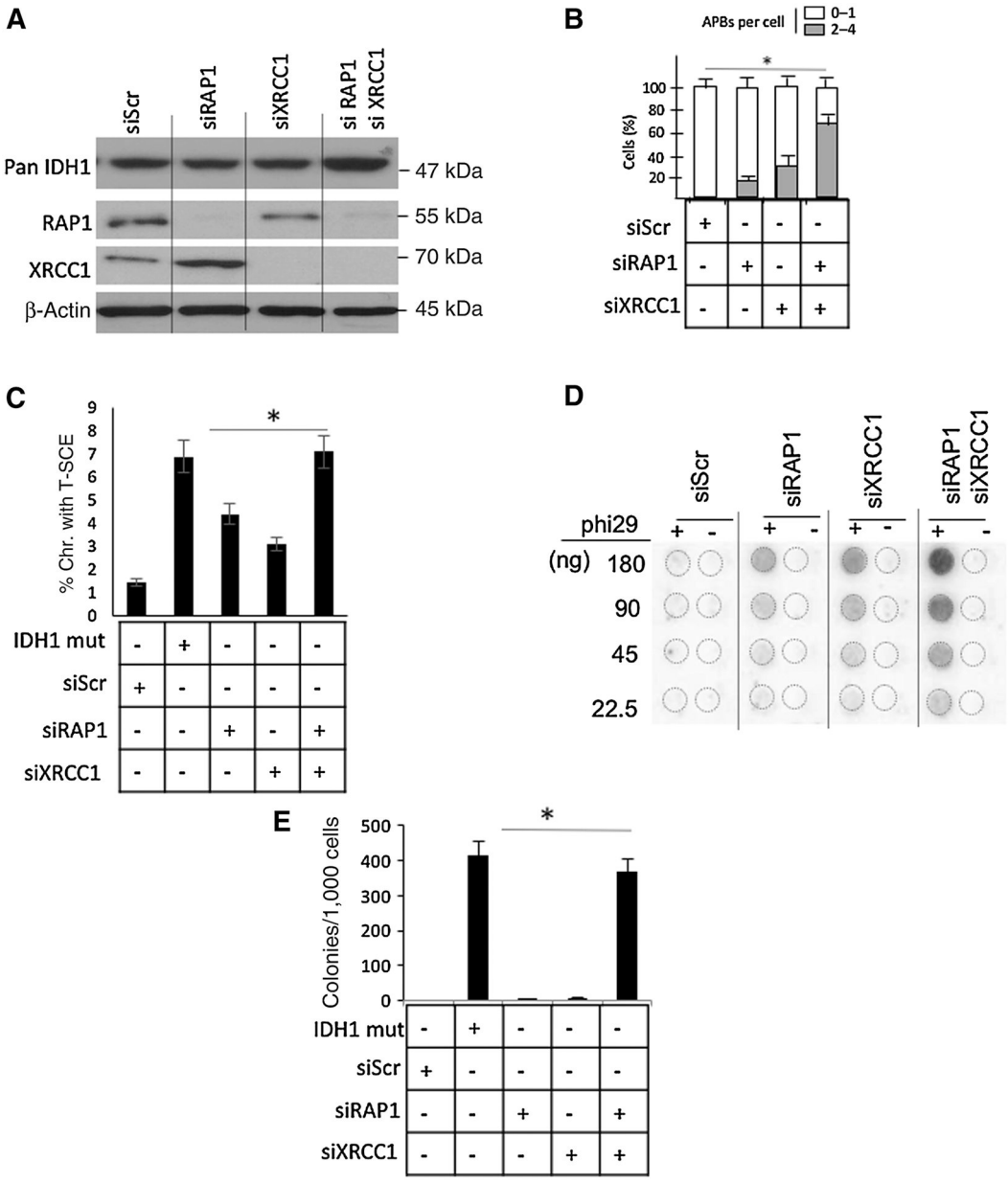

Figure 5.

siRNA-mediated suppression of RAP1 and/or XRCC1 substitutes for mutant IDH1 in driving the ALT phenotype. **A,** Western blot verification of IDH1, RAP1, XRCC1, and β-actin protein levels in *ATRX* KO-1 astrocytes transfected with scrambled siRNA or pooled siRNAs targeting RAP1, XRCC1, or both. **B,** Quantitation of the percentage of cells containing ≤1 (open box) or 2–4 (closed box) APBs per cell in >200 cells per each group described in **A**. **C,** Percentage of chromosomes with T-SCE from ATRX KO cells in **A** and also expressing blank (−) or mutant IDH1-encoding construct (+). **D,** Quantitation of C-circle DNA in cells from **A**. **E,** Number of colonies (>100 cells) that arose 28 days following plating of the cells in **D**. Except where noted, all values were derived from three independent experiments.*, $P < 0.05$.

Author Manuscript Author Manuscript Author Manuscript Author Manuscript

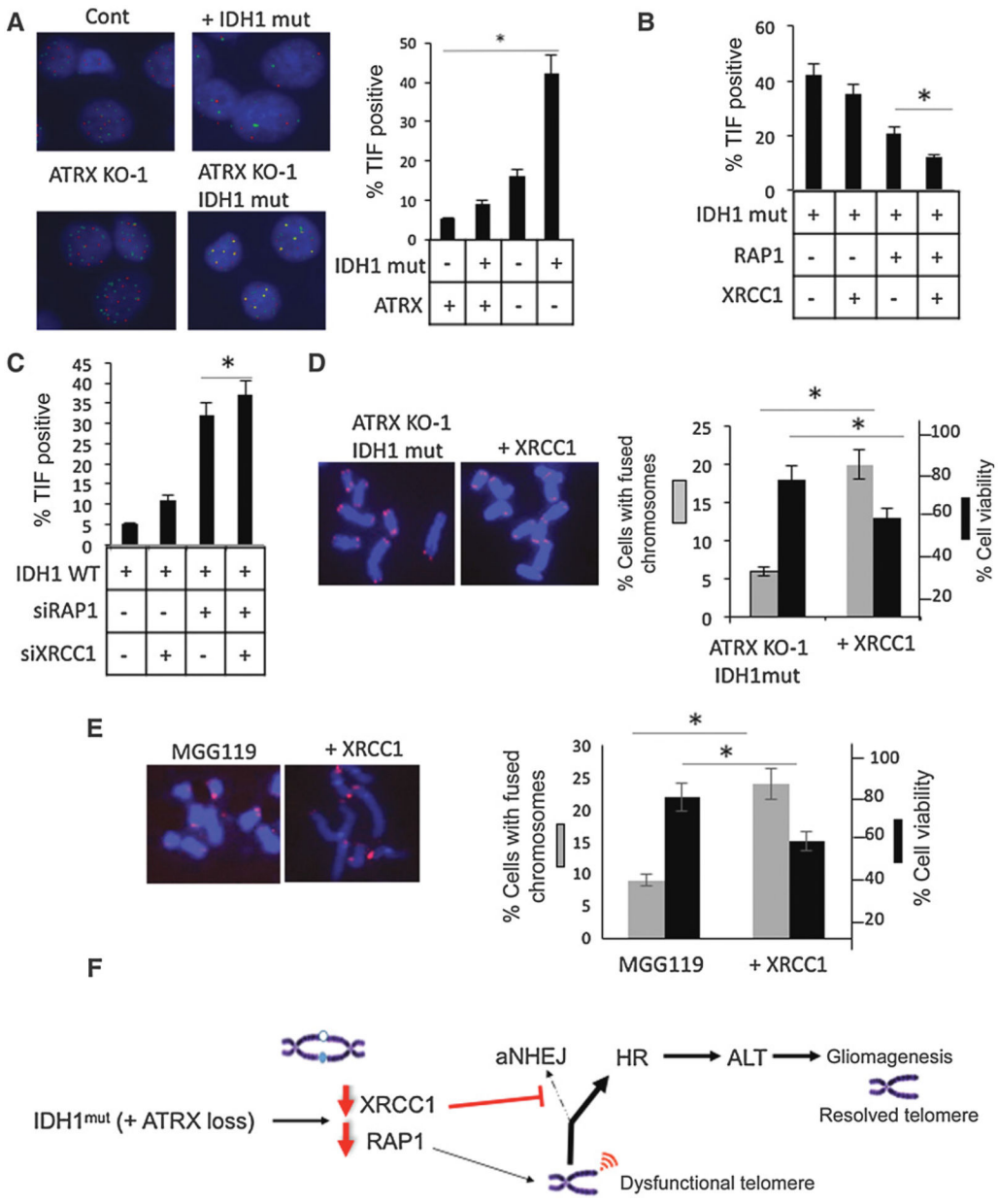

Figure 6.

Mutant IDH1-mediated downregulation of RAP1 and XRCC1 initiates telomere dysfunction and alters telomeric damage repair. **A,** Quantitation (bottom) of the percentage of control E6E7-expressing human astrocytes expressing mutant IDH1 (IDH1 mut+), subjected to CRISPR-based *ATRX* knockout, (ATRX KO-1) (ATRX−), or both and containing >2 TIFs per cell (TIF positive, yellow foci, top) based on IHC colocalization of γH2AX (red) with TRF2 (green) signal in >50 cells per group. **B,** Quantitation of the percentage of TIF-positive mutant IDH1/ATRX KO-1 cells following introduction of blank constructs or constructs encoding RAP1, XRCC1, or both. **C,** Quantitation of the percentage of TIF-positive IDH1 WT/ATRX KO-1 cells following introduction of scrambled siRNA (−) or siRNA targeting RAP1 and/or XRCC1 (+). **D** and **E,** Quantitation of the viability

Author Manuscript Author Manuscript Author Manuscript Author Manuscript

(right, dark bars) and the percentage of mutant IDH1/ATRX KO-1 (**D**) or MGG119 (**E**) cells containing ≥1 fused chromosome (right, light bars) following introduction of blank constructs or constructs encoding XRCC1, based on fluorescence microscopy analysis of >50 cells per each group (left). **F,** Schematic of the basis for mutant IDH1–mediated control of ALT. Except where noted, all values were derived from three independent experiments. *, $P < 0.05$.